Brain oscillatory correlates of visuomotor adaptive learning

Lucas Struber, Marie Baumont, Pierre-Alain Barraud, Vincent Nougier, Fabien Cignetti

Brain oscillatory correlates of visuomotor adaptive learning

Lucas Struber[1], Marie Baumont[1], Pierre-Alain Barraud[1], Vincent Nougier[1], Fabien Cignetti[1]

Univ. Grenoble Alpes, CNRS, TIMC, 38000 Grenoble, France

Corresponding author:

Lucas Struber – lucas.struber@univ-grenoble-alpes.fr

UGA Site Santé – Domaine de la Merci – Bât. Jean Roget,

38706 La Tronche

FRANCE

Abstract

Sensorimotor adaptation involves the recalibration of the mapping between motor command and sensory feedback in response to movement errors. Although adaptation operates within individual movements on a trial-to-trial basis, it can also undergo learning when adaptive responses improve over the course of many trials. Brain oscillatory activities related to these “adaptation” and “learning” processes remain unclear. The main reason for this is that previous studies principally focused on the beta band, which confined the outcome message to trial-to-trial adaptation. To provide a wider understanding of adaptive learning, we decoded visuomotor tasks with constant, random or no perturbation from EEG recordings in different bandwidths and brain regions using a multiple kernel learning approach. These different experimental tasks were intended to separate trial-to-trial adaptation from the formation of the new visuomotor mapping across trials. We found changes in EEG power in the post-movement period during the course of the visuomotor-constant rotation task, in particular an increased (i) theta power in prefrontal region, (ii) beta power in supplementary motor area, and (iii) gamma power in motor regions. Classifying the visuomotor task with constant rotation versus those with random or no rotation, we were able to relate power changes in beta band mainly to trial-to-trial adaptation to error while changes in theta band would relate rather to the learning of the new mapping. Altogether, this suggested that there is a tight relationship between modulation of the synchronization of low (theta) and higher (essentially beta) frequency oscillations in prefrontal and sensorimotor regions, respectively, and adaptive learning.

Keywords: Sensorimotor adaptive learning, Neural oscillations, Electroencephalography, Machine learning, Sparse modeling.

Highlights:

- Increases in post-movement power θ, β and γ bands underpin adaptive learning
- SMA β synchronization increase relates to trial-to-trial adaptation from errors
- Visuomotor mapping acquisition is associated with synchronized frontal θ activity

1. Introduction

Adaptation is an essential feature of motor control in which the motor command is adjusted on a trial basis to compensate for disturbances in the external environment or in the motor system itself. It involves the recalibration, or updating, of the brain's internal model that predicts the upcoming state of the motor system from the current state and the ongoing motor command. Any mismatch between the predicted motor state and the actual motor state as estimated through feedback, labelled a sensory prediction error, is used for the update of the model and the adjustment of the motor command (Diedrichsen et al., 2005; Wolpert et al., 1995; Wolpert and Miall, 1996). Adaptation can therefore be viewed as a change in the mapping that relates sensory inputs to motor outputs. Although this remapping operates fundamentally on a trial-to-trial basis, it can also engage a learning phase when sensorimotor mapping evolves over the course of many trials and stabilizes so as to become optimally tuned to specific environments and tasks (Braun et al., 2009a). This raises a fundamental question as to whether adaptation occurring on a trial basis and its improvement across trials arise through the same mechanisms or not.

A number of studies have investigated the oscillatory brain activities associated with trial-to-trial reach adaptation using paradigms of visuomotor-rotation wherein a distortion is generated between the movement and its visual representation to induce an adaptive motor response. Most of the studies focused on beta band activity, which is known to play a central role in motor control (Kilavik et al., 2013). They reported a negative correlation between movement error induced by visuomotor distortion and the amplitude of post-movement beta event-related synchronization over the sensorimotor cortex, this negative correlation being enhanced when the bias and variance of the prior errors was additionally considered (Tan et al., 2014a, 2014b). This was interpreted to reflect neural processes that evaluate the outcome of a completed movement with respect to its predicted outcome and do so in the context of errors history. Interestingly, this correlation has been reported not only when the rotational distortion remained the same across trials but also when it varied pseudo-randomly

around a mean of zero degree, that is when no learning of a new visuomotor transformation would occur (Albert et al., 2021; Diedrichsen et al., 2005; Donchin et al., 2003). This suggests that amplitude modulation of post-movement beta synchronization with respect to error size is a hallmark of trial-to-trial adaptation and do not reflect the formation of new visuomotor mapping. Recent evidence further suggested that this post-movement beta synchronization relates also to uncertainties in sensory feedback and motor feedforward estimations that determine 'how readily' movement error updates the internal model (Palmer et al., 2019; Tan et al., 2016). Hence, there seems to be a link between post-movement beta rebound, trial-to-trial adaptation, and relevance of error to update the internal model. There is also evidence that trial-to-trial adaptation triggers modulation of beta synchronization during movement planning (pre-movement), therefore linking beta synchronization to the processing of previous error and somatosensory information, both critical to the updating of motor plans (Alayrangues et al., 2019; Jahani et al., 2020; Torrecillos et al., 2015). Altogether, the above results suggest that beta synchronization prior to and following a movement could express some sort of functional polymorphism, evaluating movement error and mediating the subsequent adaptation from both motor and sensory information.

None of the above studies addressed the question of the learning occurring when a new sensorimotor mapping between feedback and motor command is acquired and becomes stable. A few studies provided some insights into this issue, examining changes in spectral power of the other oscillatory bands by comparing early and late phases of adaptation to a constant perturbation. They reported an increase of gamma power during movement execution as well as an increased power of the slower frequencies (theta and alpha) during pre-movement, especially in the parietal and frontal cortices, during the course of learning (Gentili et al., 2011; Perfetti et al., 2011; Thürer et al., 2018). Thus, rhythms outside the beta band may play a pivotal role in motor learning. Unfortunately, both adaptation and learning were intertwined in these aforementioned studies. Finally, it is worth to mention that besides spectral power, phase information is also involved in the neuronal

encoding of motor processes (Combrisson et al., 2017; Hammer et al., 2013; Jerbi et al., 2007). However, motor adaptation and learning have not yet been studied under this perspective.

In the present study, we aimed to come up with a more complete understanding of motor adaptation and learning in terms of neural oscillations and synchrony. To this end, we implemented a data-driven multivariate approach – multiple kernel learning (MKL) – that explored the different spectral features of the EEG signals – i.e. power and phase in different bandwidths and regions of interest – prior to (pre-movement) and following (post-movement) the movement during a visuomotor rotation task with constant perturbation. MKL is a powerful method that can decode states of interest from a combination of kernels (Gönen and Alapydin, 2011), such as features of the EEG signals (Schrouff et al., 2016). We examined features of adaptive behavior through an MKL model discriminating early from late stages of a visuomotor constant rotation task. We expected to find a combination of features including but not limited to pre-movement and post-movement beta power to bring information regarding adaptive behavior. However, it would have remained unclear from that modelling whether EEG features that contributed to the decision boundary were related either to trial-to-trial adaptation from errors or formation of the new visuomotor mapping since both processes occur concomitantly in a visuomotor constant rotation task. Accordingly, we also considered two other experimental conditions, including a normal movement condition that relies on the identity mapping and does not involve any adaptation, and a condition with a random rotational perturbation centered on identity mapping. In the latter, there was trial-to-trial adaptation from errors (Albert et al., 2021; Diedrichsen et al., 2005; Donchin et al., 2003), but this adaptation did not lead to the acquisition of a new sensorimotor mapping since the imposed average mapping is the identity policy as in normal movement condition (Braun et al., 2009b). MKL modelling of the constant rotation condition against these additional conditions as well as further univariate analyses provided information on the EEG

117 features most related to the trial-to-trial adaptation from errors and those relating mostly to
118 the acquisition of the new visuomotor mapping.

2. Material and methods

2.1. Participants

19 right-handed healthy volunteers (9 females and 10 males, age range: 20 – 33 years; mean ± SD age: 23 ± 3 years) participated in the study. All subjects had no history of neurological or psychiatric disorders and presented normal or corrected-to-normal vision. The study was conducted with the approval of the local ethics committee from Grenoble-Alpes University (IRB00010290-2019-02-12-60). Written informed consent was obtained from all participants.

2.2. Experimental setup

Participants were seated in front of a 27'' computer screen, 1.5 meters away, and held a joystick with their right hand, which rested on a padded arm support. An opaque panel prevented the view of the hand and forearm. Participants were equipped with a 128-electrodes cap (Biosemi©). The task, in line with previous studies (e.g. Perfetti et al., 2011; Tan et al., 2014a), consisted in performing target aiming movements with a joystick that controlled a green ball. Each movement started from the center of the screen to one of eight possible and equally spaced targets around a virtual circle (radius, 15 cm – circa 15-20° of wrist flexion). Each trial started with a 1500 to 1900 ms pre-cue period during which the eight targets were presented as red circles with transparent background. It was followed by a 1500 ms cue period during which the background of two neighbor targets became red and allowed movement planning. Then, all targets except one of the two red targets disappeared to indicate the GO signal. Participants had to reach the remaining red target as fast and as accurately as possible. Once the target was reached with a 200 ms stop inside the target or when the allowed time elapsed (> 5000 ms), a 2500 ms inter-trial interval preceded the following trial. During this interval, the green ball disappeared and only the reached target remained visible. Subjects were asked to passively let the joystick return to its initial position. The task was implemented using a custom C++ software based on Qt and Measurement Computing© libraries. The software recorded behavioral data (cursor positions) at 2048 Hz.

EEG electrodes (Biosemi system) were placed according to the international 10-20 EEG system, and acquired at 2048 Hz. Data synchronization was controlled through triggering from behavioral software.

2.3. Experimental conditions

After 50 familiarization trials, participants performed the normal movement condition (**Norm**) and then the random rotation condition (**RdmRot**), including 80 trials each. In Norm, there was a normal relationship between the display and joystick. In RdmRot, rotation angle between the cursor and the actual movement was selected randomly between -60° to +60° in step of 20° with the average angle over the 80 trials being equal to 0° (Fig. 1). Each rotation angle was presented 10 times except for the 0° angle that was presented 20 times. Finally, participants performed the condition of 60° constant rotation, which was divided in two runs of 80 trials each separated by a 2' break (**CnstRot-1** and **CnstRot-2**; Fig. 1). In all conditions, each target was visited 10 times in a random order.

Early and late stages of adaptive learning were defined as the first 30 trials of CnstRot-1 (**Early-CnstRot**) and the last 30 trials of CnstRot-2 (**Late-CnstRot**), respectively, akin to previous studies (Perfetti et al., 2011; Tan et al., 2014a). Norm, RdmRot and CnstRot-1 were used to tease apart neural correlates related either to trial-to-trial adaptation or learning of the visuomotor transformation.

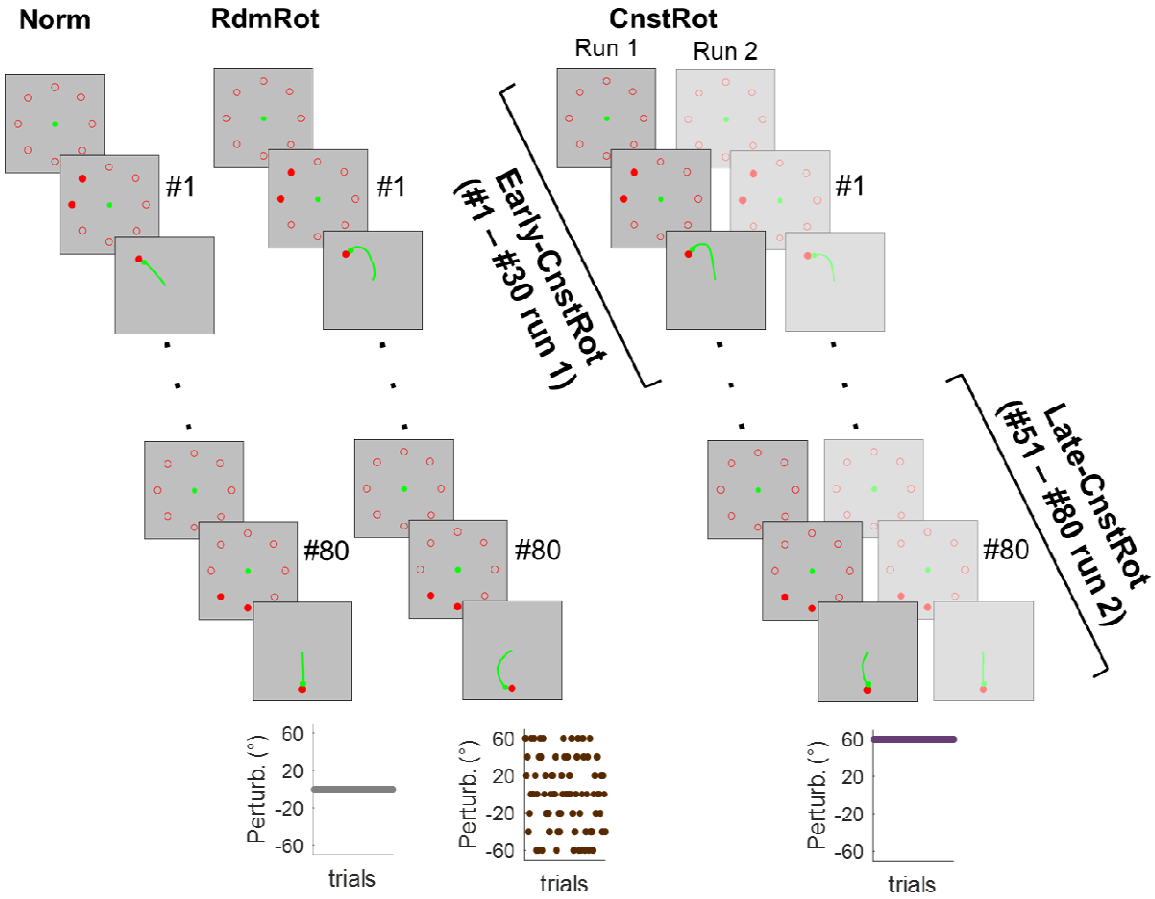

164

165 **Fig. 1.** Experimental design. Subjects started with 80 trials of Norm condition (no distortion), followed by 80 trials
166 of RdmRot condition (random rotational perturbation), then performed CnstRot condition, divided in two runs of 80
167 trials each. The first 30 trials of CnstRot-1 defined the Early-CnstRot stage while the last 30 trials of CnstRot-2
168 defined the Late-CnstRot stage. Every trial started with a pre-cue period displaying the 8 possible target locations.
169 Then, two targets lighted up during the preparation period and finally only one remained, towards which
170 participants performed their aiming movement. In Norm condition visual feedback was normal, while in RdmRot
171 and CnstRot conditions visual feedback was perturbed using random and constant perturbation, respectively.
172 Distribution of perturbations over trials are presented below each column.

173 *2.4. Behavioral analysis*

174 Behavioral analysis was performed with custom Matlab routines (R2018b). Cursor
175 positions were down-sampled at 100 Hz and then filtered through a dual low pass
176 Butterworth filter with a 20 Hz cutoff frequency. Reaction time (RT) was calculated as the
177 delay between GO signal and the time when the velocity crossed the threshold of three times
178 its SD at rest. Trials in which participants exhibited an anticipatory behavior (RT < 100ms) or

did not reach the target were excluded from further behavioral and EEG analyses. For each trial, several parameters were also computed to quantify adaptive behavior (Braun et al., 2009a; Perfetti et al., 2011; Tan et al., 2014a): (i) movement duration (MT), defined as the time elapsed between movement onset and movement termination (i.e. the moment when target was reached, after the 200ms stop within it); (ii) path length (PL), or normalized covered distance, computed as the total distance traveled by the cursor during the trial divided by the optimal path length, i.e. the length of the line connecting the starting position and the target; (iii) absolute initial angular error (AIE), defined as the absolute angle between the line connecting the initial cursor position to its position 200ms after movement onset – and before any corrective movement – and the line connecting the initial cursor position to the target; and (iv) trial-to-trial adaptation rate (AR) as estimated from state-space modelling (c.f. appendix and Tan et al., 2014a). State-space model performance was assessed using Akaike information criterion (AIC). All parameters respected normality criterion as assessed through Shapiro-Wilk tests. Accordingly, paired *t*-tests and within-subjects ANOVAs combined with Fisher LSD post-hoc tests have been used to investigate differences in mean parameters (averaged across trials). All statistical tests were performed using Statistica 10 (StatSoft©), with a level of significance set at $p < 0.05$.

2.5. EEG preprocessing

EEG data preprocessing was performed using Python and open source MNE software (https://mne.tools). First, EEG was down-sampled at 200 Hz and referenced to the average signal across all electrodes. Raw EEG signals were band-pass filtered between 1 and 80 Hz with a notch filter at 50 Hz, and detrended. All channels were visually inspected to identify bad channels which were interpolated, and blinking artifacts were rejected through ICA analysis (Delorme et al., 2007). Then, signals were epoched in two periods: 1) pre-movement, locked on GO signal, starting 2000 ms before and ending 700 ms after (to include first part of motion, before any corrective movement); 2) post-movement, locked on movement termination, starting when target was reached (200 ms before movement

termination) and ending after the 2500 ms inter-trial interval. All epochs were visually inspected to remove residual noisy epochs. “Bad epochs” based on anticipatory behavior or trials with target not reached were also excluded. To keep a large enough number of trials across participants in our main investigation between Early- and Late-CnstRot, the first 30 “good epochs” of CnstRot-1 and the last 30 “good epochs” of CnstRot-2 were considered for each participant. Regarding other conditions, 3.6 ± 3.3, 7.4 ± 7,1 and 9.4 ± 6.7 over 80 epochs were discarded in Norm, RdmRot and CnstRot-1 conditions, respectively (averaged values for pre- and post-movement epochs).

2.6. EEG time-frequency analysis

EEG time-frequency analysis was performed using Matlab (R2018b) and SPM12 toolbox (https://www.fil.ion.ucl.ac.uk/spm/). For every recording sites, each epoch was decomposed in its time frequency representation through a Hilbert transform between 1 and 80 Hz, with 1Hz non overlapping intervals and using a two-way, zero phase-lag FIR filter from EEGLAB toolbox (order 3r where r is the ratio of the sampling rate to the low-frequency cutoff of the filter, rounded down). Phase and amplitude (power) signals of the complex transform were then extracted for each frequency. This method has been shown previously to be as accurate as power estimation using Morlet wavelet (Bruns, 2004) while preserving phase information (Cohen et al., 2009; Combrisson et al., 2017; Voytek et al., 2013).

Relative EEG power changes were then calculated for Early- and Late-CnstRot as the percentage change relative to a stable baseline, by dividing the power signals at each frequency and each time point by the baseline, and then subtracting 100 from the normalized value (expressed in percent). Positive values indicated an EEG power higher than the baseline and will be reported as a synchronization while negative values will be reported as a desynchronization. The baseline was defined for each frequency as the average power during the last 500 ms of the pre-cue period, pooled across trials (i.e. one global baseline was used for the 80 trials of CnstRot-1 and CnstRot-2, before extracting Early and Late subsets). In this 500 ms period, participants were at rest, had stopped performing motion

since more than 1000 ms and were presented with only the 8 targets with transparent background. Power changes were then averaged over epochs. Then, inter-trial coherence of phase signals over epochs (ITPC) was computed. For each subject, mean ITPC value during baseline period (same period than for power) was then subtracted from ITPC signals. Typical examples of time-frequency maps (powers and ITPC averaged across subjects on central electrode Cz in Early- and Late-CnstRot) are presented on Fig. 2. Power changes and ITPC were also estimated for conditions Norm, RdmRot, CnstRot-1 the same way.

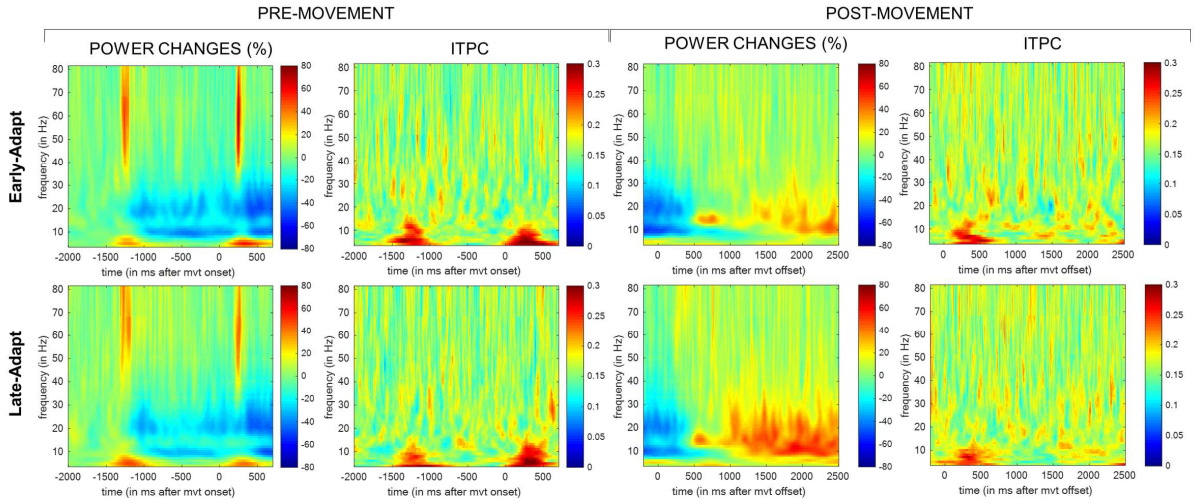

Fig. 2. Illustration of the EEG features in Early- and Late-CnstRot (on central electrode Cz). First column represents averaged power changes across subjects during pre-movement window (0 ms corresponds to GO signal). Theta (4-8 Hz) and gamma (31-80 Hz) waves presented concomitantly two synchronization peaks, after visual stimuli (immediately after the CUE signal at -1500 ms, and immediately after the GO signal at 0ms). Alpha (9-12 Hz) and beta (13-30 Hz) waves presented a desynchronization during the cue period, which became even more consistent after the go signal. Second column represents averaged ITPC across subjects during pre-movement window. Peaks of ITPC were essentially present in theta and alpha bands, right after the CUE and GO visual stimuli. Third column represents averaged power changes across subjects during post-movement window (0 ms corresponds to movement termination). Theta and gamma powers presented a slight progressive synchronization after movement. Beta and alpha powers, which were largely below the baseline at the end of the movement, presented a strong synchronization after movement, peaking between 1,5 s and 2.5 s post-movement. Fourth column represents averaged ITPC across subjects during post-movement window. A peak of ITPC was present mainly in theta and alpha bands right after the end of the movement. All these modulations are consistent with current literature (see Kilavik et al., 2013; Palmer et al., 2019; Tan et al., 2014a; Tzagarakis et al., 2010 for power modulation and Combrisson et al. 2017; Popovych et al. 2016 for ITPC).

2.7. MKL classification

MKL modelling was performed using Pronto library (http://www.mlnl.cs.ucl.ac.uk/pronto/) which is based on the SimpleMKL package (Rakotomamonjy et al., 2008). MKL is a supervised machine learning approach that simultaneously learns from different kernels (Gönen and Alapydin, 2011; Schrouff et al., 2016) in order to classify two classes, or in the present study, conditions. MKL uses the set of inputs to build kernels representing pair-wise similarity between observations (dot product in Pronto). Then, a support vector machine (SVM; Cortes and Vapnik 1995) allows to define a decision boundary, discriminating between classes, for each kernel. To determine this boundary, model parameters w_m, representing the contribution of each feature (unitary element of each input, e.g. time point) is optimized. Each decision boundary (one per kernel) is then weighted by a parameter d_m to define a global decision boundary. These two steps are implemented recursively in an optimization procedure, with a L1-norm sparsity constraint on the d_m vector, encouraging a sparse selection of non-null kernel contributions. Final kernel contributions d_m and feature contribution w_m are then retrieved (Fig. 3). However, contrary to d_m, w_m are not sparse in MKL modelling, meaning that every features contributed to the model. As such, interpreting w_m is complex and raises several issues (Haynes, 2015; Schrouff et al., 2016), so that we preferred focusing our interpretation of the results on the kernel contributions d_m. MKL algorithm is based on SVM models, which includes a soft-margin hyper-parameter C. This hyper-parameter allows more or less misclassifications during training, affecting SVM decision boundary. To optimize this hyper-parameter, we performed a nested cross-validation scheme in which an inner loop was used for hyper-parameter selection leading to the highest model performance whereas an outer loop used the selected hyper-parameter to assess the performance. This optimization procedure selected C = 1 for around 80% of the folds in all our MKL implementations and C = 0.1 or 10 for the remaining ones. Thus, we chose to set C = 1 in order to keep the same hyper-parameter across all folds.

283 In the present study, for every two-class classification, MKL was fed with input signals
284 representing either temporal band-related power changes or temporal band-related ITPC, in
285 the four main bands of interest (theta: 4-8 Hz, alpha: 9-12 Hz, beta: 13-30 Hz and gamma:
286 31-80 Hz). A region-of-interest (ROI) approach was used to limit influence of highly
287 correlated data, averaging power changes and ITPC signals within different ROIs. ROIs
288 definitions and examples of averaged (across subjects and ROIs) temporal band-related
289 power changes are depicted in the left panel of Fig. 3. From a technical standpoint, input
290 signals were converted into nifti files in order to fit the Pronto imaging toolbox. Thus, 44
291 kernels (11 ROIs x 4 bands) of size 38x38 (19 subjects x 2 conditions) were built for each
292 classification. To ensure that the scale of each kernel did not interfere in modelling, all
293 kernels were mean-centered and normalized. Adaptive learning as a whole was decoded
294 classifying Early- against Late-CnstRot for power changes and ITPC signals and during pre-
295 and post-movement separately, leading to four main MKL implementations. We did not
296 include pre- and post-movement periods as well as power changes and ITPC signals in the
297 same model to avoid over-parametrization.

298 When a classification was significant (see section 2.8.), further MKL classifications
299 between conditions were performed to investigate more accurately the role of the identified
300 kernels (CnstRot-1 vs. Norm, CnstRot-1 vs. RdmRot, and Norm vs. RdmRot). CnstRot-2 was
301 discarded from these further classifications due to its intermediate position between CnstRot-
302 1 and Norm both in term of error size and acquisition of the new mapping.

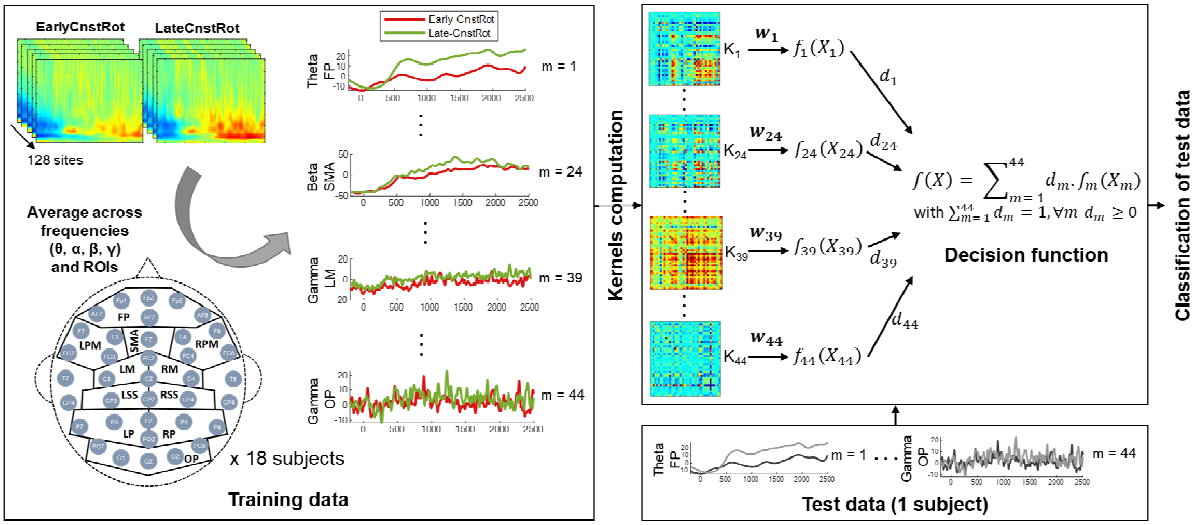

Fig. 3. Illustration of multiple kernel learning modelling procedure for Early- vs. Late-CnstRot. For each subject but one, and for each electrode, time-frequency power (or ITPC) maps were computed in both Early- and Late-CnstRot stages. These maps were then averaged across frequencies (in theta, alpha, beta and gamma bands) and over predefined regions of interest (ROIs) to define the 44 feature vectors in the two conditions (labels of the feature vectors are the conditions). ROIs were defined as showed on head map on the left side of the figure. For each region/band couple, a linear kernel Km, representing the pair-wise similarity between features vectors of both conditions across subjects was built (m = 1 … 44). All kernels and their associated labels were then used to train the model. First, features contributions w_m are estimated to define a decision function f_m per kernel. The weight of each decision function, d_m, is then estimated to provide a final decision function f(x). These two steps are implemented recursively in an optimization procedure, leading to a sparse selection of non-null kernel contributions. The model was then applied to test data (feature vectors of the 19th subject without labels) to obtain associated predicted conditions. This whole process was repeated as many times as there were subjects, excluding a different subject each time to assess accuracy of the model. Abbreviations: FP: frontal pole, LPM: left premotor, SMA: supplementary motor area, RPM: right premotor area, LM: left motor, RM: right motor, LSS: left somatosensory, RSS: right somatosensory, LP: left parietal, RP: right parietal, OP: occipital pole.

2.8. Decoding performance

Performances of the MKL models were assessed using a “leave-one-subject-per-class-out” cross validation scheme. This scheme is the best choice when subjects in different classes are correlated (i.e. within subject design), keeping testing and training sets independent. Indeed, to ensure proper cross-validation, it is crucial that correlated information (here the same subject) is not present both in the train and test sets. Such a

dependency would lead to “leakage” and over-optimistic model performance. In our design, the only way to keep testing and training sets completely independent was to split our data by subjects. Thus, each model was trained using all subjects with their corresponding labels (here conditions) except one, and used to predict the labels of the subject left out. This process was repeated as many times as there were subjects. Total accuracy (TA) and class accuracy (CA) were subsequently obtained as the total number of correctly classified test samples divided by the total number of test samples, irrespective of class for TA and for a given class for CA.

Since training sets were not independent across folds (overlapping of training data between folds), the use of any parametric tests was excluded to assess the statistical significance (Noirhomme et al., 2014; Pereira et al., 2009). P-value associated to each performance measure was estimated using a 1000-permutation testing framework in which cross-validation and accuracy were recomputed after randomly shuffling training labels (Ojala and Garriga, 2010). The level of significance was set at $p < 0.05$ for TA.

2.9. Univariate analyses

We conducted further analyses on the kernels that were most contributing to the MKL models in order to refine the distinction between neural processes most related to trial-to-trial adaptation from those most linked to the learning of the new visuomotor transformation. It is however important to mention that these selective analyses were run on a subset of the kernels and as such suffered double dipping (Kriegeskorte et al., 2009). Accordingly, univariate analyses served to make interpretation of MKL models easier, but should not be considered as hypothesis testing *per se.*

In this perspective, *t*-tests and one-way ANOVAs were used to evaluate differences of average power or PLV amplitude over time in the kernels that contributed the most to distinguish between Early-CnstRot and Late-CnstRot as well as between Norm, RdmRot and CnstRot-1. Also, we assessed the correlation between this average amplitude and error size

in CnstRot-1 and RdmRot conditions. To this end, for each condition, kernel and subject, trials were grouped into 8 bins according to the size of the AIE, and Fisher *r-to-z* transform was computed between bin's order and the average amplitude signal in the post-movement period. Significance of the correlations were afterwards examined using one sample *t*-tests. In kernels associated with trial-to-trial adaptation from errors, correlation between error size and average magnitude should be present in both RdmRot and CnstRot-1 conditions while in kernels associated with learning of the new visuomotor transformation, this correlation should be present only in CnstRot-1 condition. Indeed in the latter, decrease of errors should more or less match with time course of the experiment and the increased level of acquisition of the transformation.

3. Results

3.1. Decoding early from late stages of visuomotor-constant rotation task

3.1.1. Behavioral results

Paired *t*-test on RT between Early- and Late-CnstRot was not significant ($p = 0.67$), indicating that the level of readiness remained similar during the task (Mean ± SD RT: 0.36 ± 0.02s; Fig. 4). Other behavioral measures showed that subjects adapted to the constant rotational perturbation. Both the AIE (41.0° ± 2.1 to 22.0° ± 1.2; $p < 0.001$) and the AR (0.0230 ± 0.004 to 0.009 ± 0.002; $p < 0.001$) decreased from Early- to Late-CnstRot. MT and PL followed the same pattern, decreasing significantly from Early- to Late-CnstRot (Early-CnstRot: MT = 1.15s ± 0.05 and PL = 1.70 ± 0.05; Late-CnstRot: MT = 0.89s ± 0.04 and PL = 1.36 ± 0.03; $p < 0.001$). Nevertheless, although the level of adaptation was largely improved in Late-CnstRot, it was still not comparable to the level of Norm condition (Fig. 4). Hence, subjects adapted to the new visuomotor transformation although room for improvement remained.

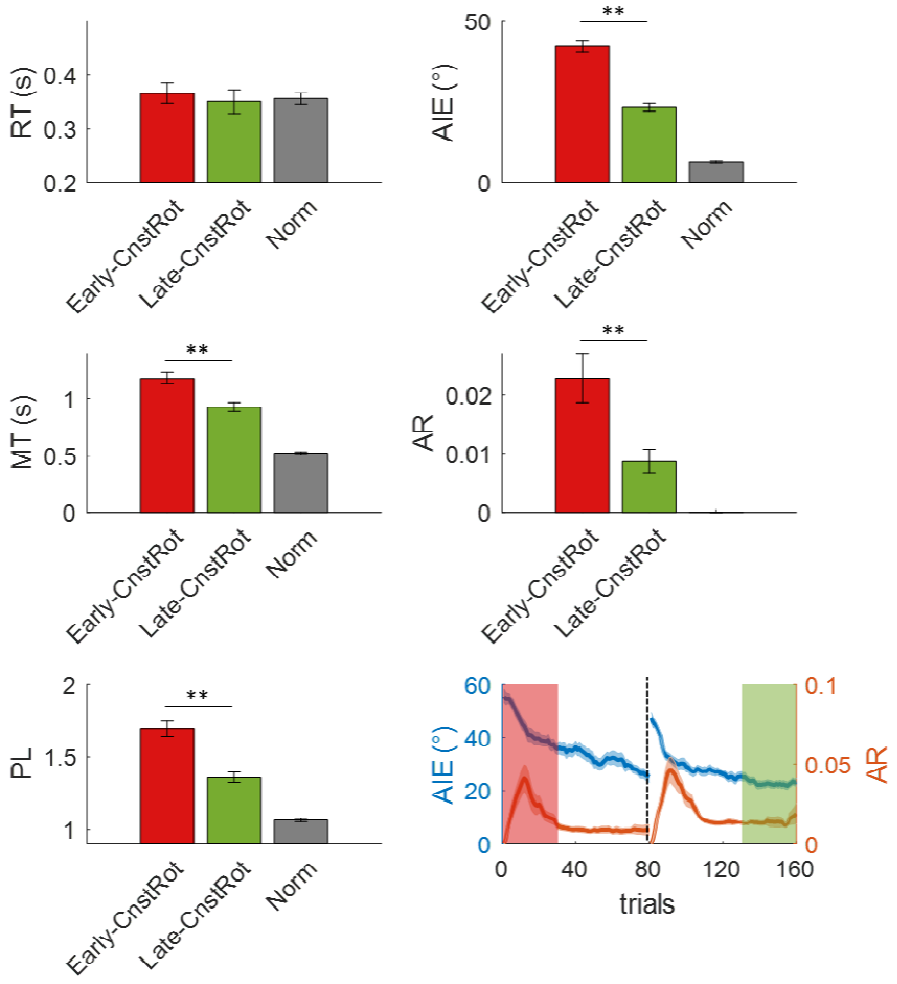

Fig. 4. Kinematic results during visuomotor-constant rotation task. While reaction time (RT) remained stable, movement time (MT), initial angular error (AIE), normalized path length (PL) and adaptation rate (AR) decreased during the course of adaptation. Bottom right panel depicts evolution of AIE and AR during the course of CnstRot condition. Values in Norm condition are provided as reference. Values are mean ± SE. **p<0.01 in *t*-tests.

3.1.2. MKL modelling

The main objective of the study was to decode the process of adaptive learning based on EEG spectral features. To do so, we ran four MKL models aiming at classifying early (Early-CnstRot) and late (Late-CnstRot) stages of a constant perturbation condition based on power and ITPC from multiple frequency bands and cortical regions during pre- and post-movement. The MKL model whose kernels were built from power of the different band/regions couples in post-movement period was statistically significant (TA = 86.84%, p = 0.002; CA = 84.21% and 89.47%, p = 0.004 and p = 0.002 for Early- and Late-CnstRot,

388 respectively). MKL classification based on kernels built from power in pre-movement did not
389 distinguish the two classes (TA = 65.79%, p = 0.11). As for ITPC-based modelling, both pre-
390 and post-movement classifications failed to dissociate Early- from Late-CnstRot (TA =
391 60.53% and 26.32%, p = 0.26 and p = 0.97 for pre- and post-movement, respectively). These
392 results suggested that motor adaptation and learning (on 160 trials) was related to
393 modulation of brain waves' power in post-movement, only.

394 Kernel contribution to the MKL model of Early- vs. Late-CnstRot based on power in
395 post-movement was assessed in terms of frequency bands, ROIs, and ROI for each
396 frequency band (a.k.a. ROI×band), as depicted in Fig. 5. Three frequency bands actively
397 participated to the classification, including the theta, beta and gamma bands with a
398 contribution of 29.4%, 18.6% and 51.7%, respectively (Fig. 5A). ROIs that contributed the
399 most to the MKL model were mainly distributed over frontal and central regions (e.g., d_{FP} =
400 20.5%, d_{RPM} = 11.6%, d_{SMA} = 17.9%, d_{RM} = 10.3%, d_{LM} = 20.6%; Fig. 5B). Interestingly, when
401 looking at ROI×band kernels (Fig. 5C), it appeared that frontal and premotor cortices were
402 related to the theta band (d_{FP_theta} = 19.9%, d_{RPM_theta} = 9.0%), supplementary motor area to
403 the beta band (d_{SMA_beta} = 17.9%), whereas motor and post-central cortices were associated
404 with the gamma band (d_{RM_gamma} = 10.3%, d_{LM_gamma} = 19.6%, d_{LP_gamma} = 9.8%).

405 Power changes (averaged across subjects) in post-movement window are represented
406 in Fig. 5C for the three main contributing ROI×band-specific kernels (FP theta, SMA beta and
407 LM gamma, which accounted together for 57.4% of the total contribution) to qualitatively
408 examine their evolution between Early- and Late-CnstRot. For FP theta, power was roughly
409 at a baseline level in Early-CnstRot and became positive in Late-CnstRot, which reflected
410 occurrence of post-movement theta band synchronization with adaptation. A similar trend
411 was found for LM gamma, also indicating the occurrence of a post-movement
412 synchronization in this frequency band during the course of adaptive learning. Regarding
413 SMA beta, there was an increased post-movement rebound, or equivalently post-movement
414 synchronization, from Early- to Late-CnstRot. These trends were confirmed by *t*-tests on

415 average post-movement synchronization between Early- and Late-CnstRot in each kernels
416 ($p < 0.001$, $p = 0.003$ and $p = 0.03$ for FP theta, SM beta and LM gamma, respectively).

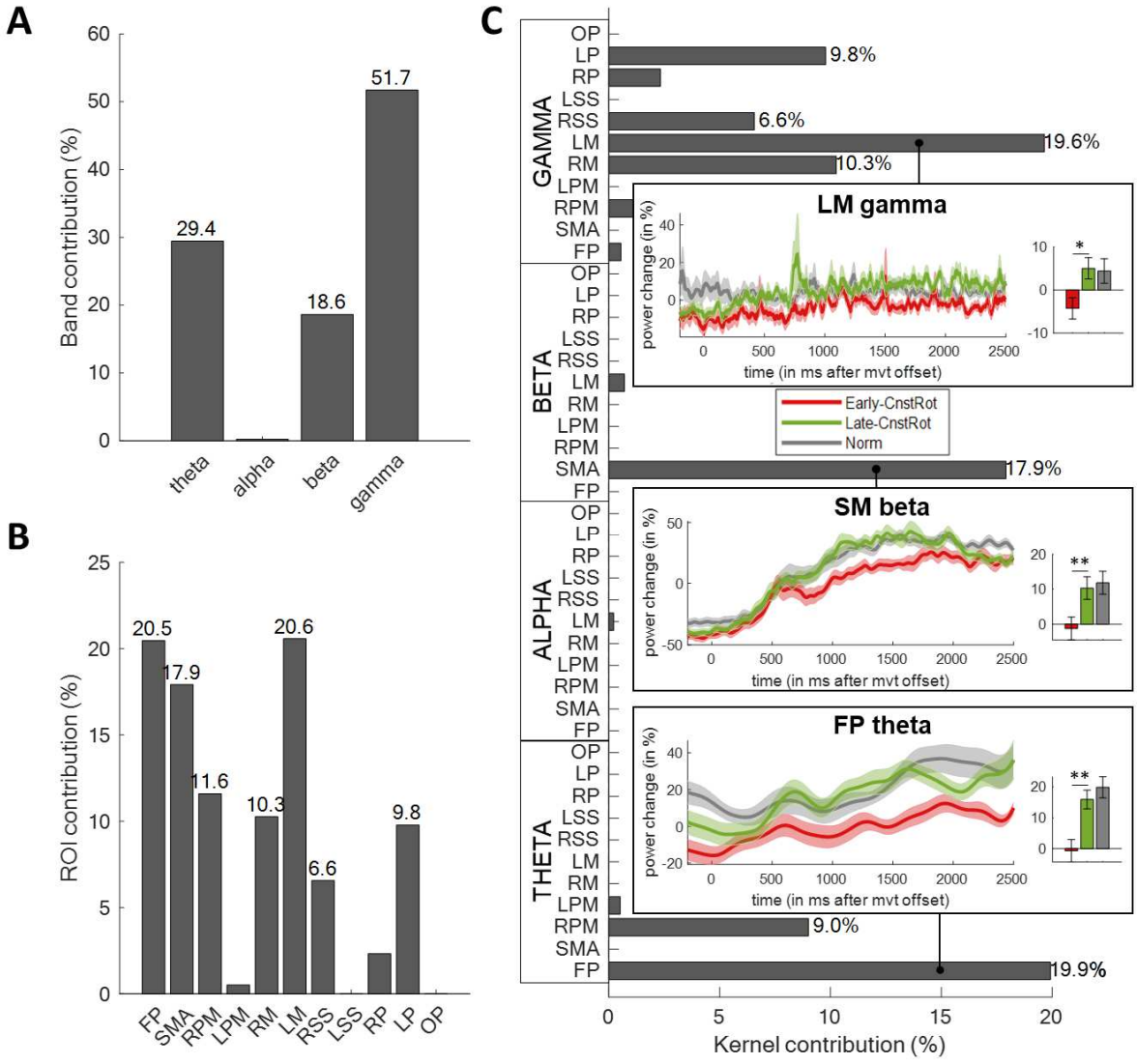

417

418 **Fig. 5.** Kernel contributions to Early- vs. Late-CnstRot MKL modelling and power changes of the most contributing
419 kernels. (A) Contribution of each band, shared between theta, beta and gamma. (B) Contribution of each ROI,
420 distributed mainly across frontal, premotor and motor cortices. (C) Contribution of each kernel (band/ROI couple),
421 revealing three main clusters of contribution: frontal to premotor theta oscillations, supplementary motor area beta
422 oscillations and motor/post-central gamma oscillations. Averaged power changes across subjects of the three
423 main contributing kernels are represented for Early- (red) and Late-CnstRot (green), as well as mean ± SE values
424 (over the time period - 0 ms corresponds to movement termination), showing the increase of post-movement
425 synchronization in these three kernels during adaptation. Averaged power changes across and mean values in
426 Norm (grey) condition are provided as reference. *p<0.05, **p<0.01 in t-tests.

3.2. Decoding conditions with (either constant or random) and without visuomotor rotation

3.2.1. Behavioral results

Within-subjects ANOVA did not reveal ($p = 0.94$) any RT difference between Norm, RdmRot and CnstRot-1 (Mean ± SD RT: 0.36 ± 0.01s; Fig. 6), suggesting a comparable level of readiness in all conditions. The other ANOVAs demonstrated an effect of condition on MT ($F_{2,54} = 84.5$; $p < 0.001$), AIE ($F_{2,54} = 143.4$; $p < 0.001$) and PL ($F_{2,54} = 49.0$; $p < 0.001$). Fisher LSD post-hoc testing revealed lower values in Norm as compared to the other two conditions on MT (Norm: 0.49s ± 0.01, RdmRot: 1.07s ± 0.03, CnstRot-1: 1.09s ± 0.04, $p < 0.001$), PL (Norm: 1.06 ± 0.01, RdmRot: 1.55 ± 0.03, CnstRot-1: 1.56 ± 0.05, $p < 0.001$) and AIE (Norm: 6.4° ± 0.2, RdmRot: 34.1° ± 0.4, CnstRot-1: AIE = 36.1° ± 1.8, $p < 0.001$). Interestingly, post-hoc testing did not reveal any difference on those parameters between RdmRot and CnstRot-1 ($p = 0.55$, $p = 0.86$ and $p = 0.27$ for MT, PL and AIE respectively). Likewise, *t*-test on AR between RdmRot and CnstRot-1 did not reveal any statistical difference (RdmRot: 0.010 ± 0.005, CnstRot-1: 0.014 ± 0.002, $p = 0.34$), with an equivalent state-space model performance (AIC RdmRot: 380.1 ± 15.1, AIC CnstRot-1: 366.1 ± 12.5, $p = 0.32$). Thus, Norm and RdmRot differed regarding error size and adaptation rate whereas RdmRot and CnstRot-1 did not. As such, any difference between Norm and RdmRot provided information on trial-to-trial adaptation after exposure to errors, whereas difference between RdmRot and CnstRot-1 informed on “cumulative” learning of the new visuomotor transformation. The difference between Norm and CnstRot-1 embedded both processes.

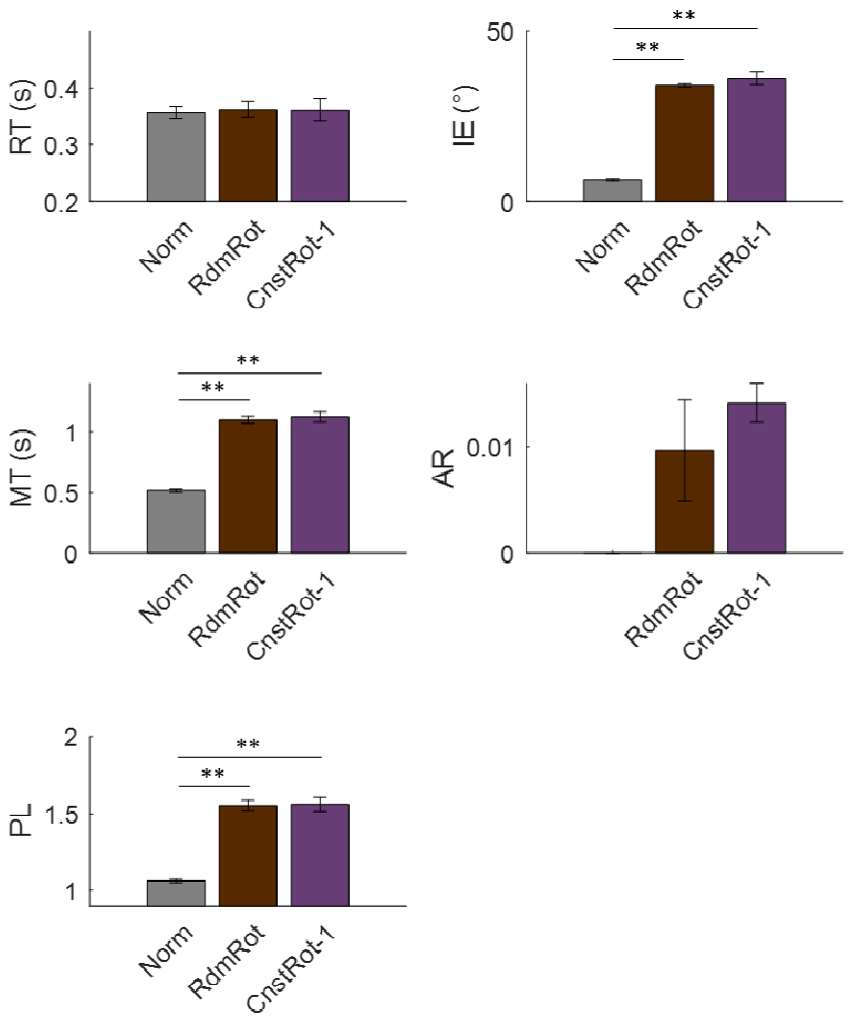

447

448 **Fig. 6.** Kinematic comparison of the different experimental conditions. Reaction time (RT) was stable across
449 conditions. Movement time (MT), Initial angular error (AIE), and Normalized path length (PL), were similar
450 between RdmRot and CnstRot-1 conditions, and lower in Norm condition. Adaptation rate (AR) was similar
451 between RdmRot and CnstRot-1. Values are mean ± SE. *p<0.05, **p<0.01 in post-hoc Fisher LSD tests.

452 *3.2.2. MKL modelling*

453 We implemented three MKL models to uncover which of the post-movement power-
454 based kernels that decoded early from late stages of CnstRot condition were most
455 associated with trial-to-trial adaptation from errors or cumulative learning of the new
456 visuomotor transformation: Norm vs. CnstRot-1, Norm vs. RdmRot and CnstRot-1 vs.
457 RdmRot.

458 The MKL model Norm vs. CnstRot-1 showed a significant discrimination between the
459 two conditions (TA = 82%, p = 0.002; CA = 79% and 84%, p = 0.02 and 0.006 for Norm and
460 CnstRot-1, respectively). The contribution vector d_m revealed a set of kernels that were
461 equivalent to those of the classification of Early- against Late-CnstRot, with post-movement
462 theta power in frontal pole and premotor areas, beta power in supplementary motor area and
463 gamma power in motor and parietal areas most contributing to the decision function. There
464 was also a noticeable difference (compared to Early- vs. Late-CnstRot) in the balance of the
465 kernel contribution to the decision boundary, with more contributory signal in the theta band
466 than in the higher-frequency beta and gamma bands (d_{theta} = 66.3%, d_{beta} = 10.9% and d_{gamma}
467 = 14.6%; Fig. 7A). Qualitatively, all contributing kernels showed weaker power in CnstRot-1
468 compared to Norm (Fig. 7A). Given that Norm and CnstRot differed both in terms of
469 movement error and level of acquisition of the imposed mapping, these results supported
470 once again the idea that post-movement theta synchronization in frontal pole and premotor
471 regions, as well as beta synchronization in SMA, and gamma synchronization in motor-
472 related and parietal regions were related to adaptive learning.

473 The MKL model Norm vs. RdmRot led to a significant classification of the conditions
474 (TA = 74%, p = 0.016; CA = 63% and 84%, p = 0.2188 and 0.006 for Norm and RdmRot
475 respectively). Post-movement beta power in the supplementary motor area and gamma
476 power in motor to parietal regions mainly contributed to the model (d_{beta} = 46.2% and d_{gamma} =
477 40.6%; Fig. 7B). Contribution of theta band was still present, but to a much lesser extent than
478 the higher-frequency bands (d_{theta} = 11.9%), and emerged from parietal areas and not from
479 prefrontal areas as in the case of Early- vs Late-CnstRot MKL model. Accordingly, this result
480 suggested that both supplementary motor area beta power and motor to parietal areas
481 gamma power after movement completion principally reflected trial-to-trial adaptation from
482 errors. The observed lower amplitude of post-movement beta and gamma power in RdmRot
483 compared to Norm suggested an inverse relationship between error and post-movement
484 high-frequency band synchronization (Fig. 7B). This finding also shed new light on frontal

485 and premotor theta power strongly involved in the classification of both Early- vs. Late-
486 CnstRot and Norm vs. CnstRot-1 which may be rather associated with the level of acquisition
487 of the sensorimotor mapping. However, this conclusion on the relationship between post-
488 movement frontal theta band synchronization and update of the mapping lacks direct
489 demonstration as the MKL model RdmRot vs. CnstRot-1 did not show a significant result (TA
490 = 50.00%; p = 0.55).

491 *3.2.3. Univariate analyses*

492 Further comparisons between kernels identified through above mentioned MKL models
493 are presented in Fig 7C. For FP theta kernel, within-subjects ANOVA revealed an effect of
494 condition on mean post-movement power ($F_{3,54}$ = 5.25; p = 0.003). Post-hoc testing revealed
495 a lower power in CnstRot-1 compared with the other conditions (p < 0.001 and p = 0.03 in
496 comparison to Norm and RdmRot respectively), while Norm and RdmRot conditions
497 presented similar levels (p = 0.08). These differences suggested that increase in post-
498 movement FP theta mean power would reflect principally the level of acquisition of the new
499 mapping. Indeed, although the acquisition of the new mapping was underway in CnstRot-1 it
500 remained largely incomplete while it was complete in Norm and RdmRot condition and
501 corresponded to the identity mapping (i.e. $< \emptyset >= 0°$).

502 Regarding SMA beta kernel, within-subjects ANOVA also demonstrated an effect of
503 condition ($F_{3,54}$ = 5.10; p = 0.004). Post-hoc testing revealed a larger mean power in Norm
504 compared to RdmRot and CnstRot-1 (p = 0.001 and 0.003 respectively). These differences,
505 in addition to the absence of significant difference between CnstRot-1 and RdmRot,
506 corroborated our guess that mean amplitude of post-movement SMA beta reflected trial-to-
507 trial adaptation from errors, which was similar in CnstRot-1 and RdmRot. On the other hand,
508 within-subjects ANOVA for LM gamma kernel did not reveal any difference between
509 conditions (p = 0.20). Hence, this extra analysis remained inconclusive on whether post-
510 movement power in LM gamma relate rather to trial-to-trial adaptation or cumulative learning
511 of the new mapping.

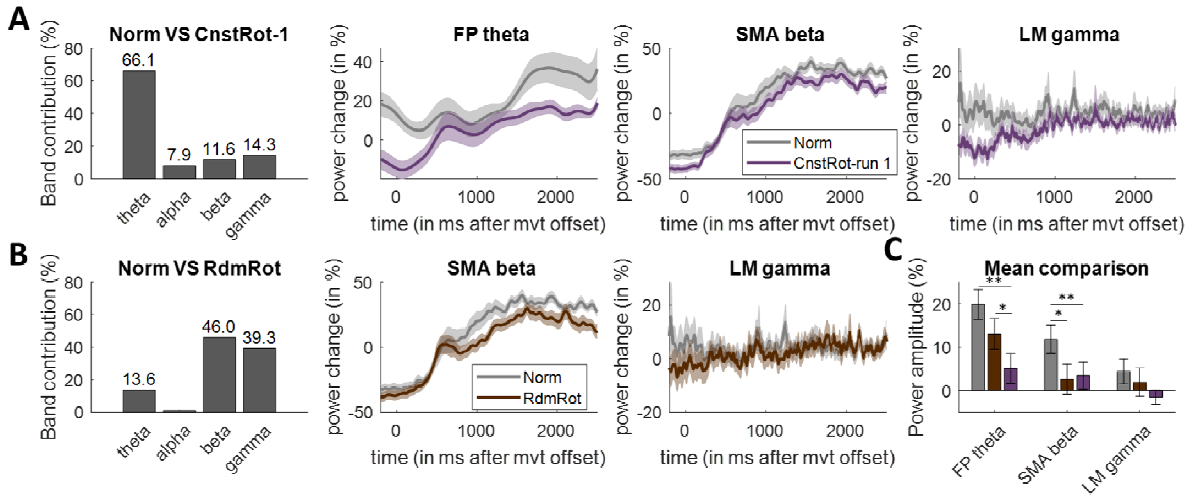

512

513 **Fig. 7.** Results of extra MKL models. (A) Norm vs. CnstRot-1 model: Theta, beta and gamma bands mainly
514 contributed to the model (as in Early- vs. Late-Adapt model), although with a dominance of the theta contribution.
515 Main identified kernels qualitatively showed a larger power in Norm compared to CnstRot-1. This supported the
516 implication of these three kernels in both movement error and acquisition of the new mapping. (B) Norm vs.
517 RdmRot model: beta and gamma bands mainly contributed to the model. SMA beta and LM gamma kernels
518 showed a larger power in Norm compared to RdmRot, suggesting that these kernels were principally related to
519 trial-to-trial adaptation. Note that theta band was also identified as contributing to the model. However, further
520 analysis revealed a parietal contribution on it, which differed from the theta contribution in frontal areas of the
521 Early- vs. Late-CnstRot MKL model. (C) Mean postmovement power for the three main contributing kernels in all
522 conditions. CnstRot-1 postmovement average power was lower than both Norm and RdmRot powers in FP theta
523 kernel suggesting a relationship with level of acquisition of the new transformation. Furthermore, Norm
524 postmovement average power was lower than both RdmRot and CnstRot-1 levels in SMA beta kernel, relating
525 beta modulation to the adaptation process. These extra-analyses remained inconclusive regarding LM gamma
526 kernel. *p<0.05, **p<0.01 in post-hoc Fisher LSD tests.

527 Finally, we found significant correlations between bin's order (sorted according to
528 decreasing error size) and mean post-movement power for SMA beta in both CnstRot-1 and
529 RdmRot conditions ($R = 0.38 \pm 0.03$, $p = 0.006$ and $R = 0.24 \pm 0.03$, $p = 0.04$ respectively).
530 The smaller the error, the larger the mean post-movement power in SMA in the two
531 conditions. Thus, post-movement power in SMA was modulated by error size. There was
532 also a significant correlation for FP theta in CnstRot-1, but not in RdmRot ($R = 0.23 \pm 0.02$, p
533 $= 0.03$ and $R = 0.12 \pm 0.03$, $p = 0.28$). This absence of relationship in FP theta for RdmRot

condition indicated that postmovement theta modulation during adaptive learning rather reflected the formation of the new mapping. Regarding LM gamma kernel, power did not correlate with bins of decreasing error size in both conditions.

4. Discussion

The aim of this study was to come up with a more complete characterization of adaptive learning in terms of neural oscillations and synchrony of distributed brain regions, and try to tease apart two subtending processes, namely trial-to-trial adaptation from errors and cumulative learning of a new sensorimotor mapping. Our main MKL model indicated that post-movement synchronization of beta oscillations in supplementary motor area, gamma oscillations in motor to parietal regions and low-frequency, theta, oscillations in (pre)frontal regions contributed to adaptive learning. Further discriminant models suggested that higher-frequency – beta and gamma – synchrony in motor-related regions was associated rather to trial-to-trial adaptation, while low-frequency synchrony in (pre)frontal regions rather informed on acquisition of the new mapping. Univariate analyses also pointed in the same direction, except for the gamma band. Modulation of SMA synchrony in the beta band was similar when facing both constant and random perturbations, in particular with a power that increased as a function of decreasing error size. This reinforced the idea that post-movement beta power relates to error processing that instantiates trial-to-trial adaptation. Inversely, modulation of frontal synchrony in the theta band differed between the conditions of constant and random perturbations, with the latter condition being similar to the condition with normal movements. Increased theta power during the course of adaptation seems therefore to be a hallmark of the acquisition of a new visuomotor mapping. Finally, univariate outcomes were inconclusive concerning the link between post-movement gamma synchronization and either trial-to-trial adaptation or cumulative learning.

An important result was the increase in post-movement beta synchronization during the constant rotation task to a level comparable to normal condition. Hence, there was an attenuation of post-movement beta power at the beginning of adaptive learning, that tended to disappear as learning progressed, confirming earlier results (Palmer et al., 2019; Tan et al., 2014a, 2014b). Furthermore, we were able to relate these brain oscillatory changes to the adaptation process that occurs independently of cumulative learning of the new

564 sensorimotor mapping, thus linking them to the processing of a completed movement with
565 respect to its predicted outcome. This complements previous results which specifically linked
566 post-movement beta synchronization to movement error and confidence in internal model
567 estimations in motor and somatosensory cortices, suggesting that post-movement beta
568 synchronization decrease could signal a need for adaptation of the motor output (Palmer et
569 al., 2019; Tan et al., 2016). The topography of our result was different, being confined mainly
570 to SMA. An explanation for this topographic discrepancy is that we let the MKL to select the
571 most discriminating regions (i.e. data-driven approach) while the above mentioned studies
572 did an a priori choice with respect to EEG channels of interest (i.e. model-based approach).
573 Accordingly, adaptation from errors may be mainly mediated through SMA although other
574 sensorimotor regions also likely contribute to it. Interestingly, it is acknowledged that
575 synchronized beta oscillations bind multiple sensorimotor regions into a large-scale network
576 during motor behavior (Brovelli et al., 2004). This also remains true with subcortical areas
577 such as the subthalamic nucleus whose beta power increases in coherence with that of the
578 sensorimotor cortex after movement offset (Tan et al., 2014b). Consequently, beta oscillatory
579 activity may be synchronized between different sensorimotor cortical (SMA, motor,
580 somatosensory) and subcortical areas to process movement error and mediates subsequent
581 adaptation. In addition, our result strengthens the indication that regions of the medial frontal
582 cortex, especially the SMA and the dorsal anterior cingulate cortex (dACC), play a critical
583 role in processing errors and evaluating the outcomes of action (Amiez et al., 2012; Bonini et
584 al., 2014; Botvinick et al., 2004; Ridderinkhof et al., 2004). It is clear that the oscillatory
585 activity we reported here is not limited to SMA but also includes influence from the dACC
586 which lies underneath. Finally, we did not find relationship between adaptive features and
587 pre-movement beta synchronization as suggested before (Torrecillos et al., 2015). This
588 discrepancy may reside in the fact that premovement period could be more involved in the
589 integration of somatosensory information (Alayrangues et al., 2019) than in processing of
590 sensory prediction error, that are both essential for adaptive update of the upcoming

591 movement. Thus, we propose that post-movement modulation of beta power reflects sensory
592 error processing and subsequent signal that engages internal model update.

593 Our MKL main result also revealed that synchronization in post-central regions within
594 the gamma band during the post-movement period was involved in overall adaptive learning.
595 However, we failed to reach a clear conclusion about the particular process that was
596 encoded through gamma modulation. At the most, our study suggested that post-movement
597 gamma modulation would relate to error processing that triggers adaptation on a trial basis
598 rather than to learning a new visuomotor transformation. This would suggest that gamma
599 oscillations may not only serve the function of encoding afferent (proprioceptive) feedback
600 and properties (e.g. velocity, effort, force level) of the movement reported in previous motor
601 control studies (Muthukumaraswamy 2010; see also Nowak et al., 2018 for review and
602 references therein). Besides, the involvement of gamma oscillations in processing of action
603 outcome that triggers motor adaptation recalls previous reports that found a role of gamma
604 oscillations in encoding reward outcomes for adapting to challenging tasks (Quilodran et al.,
605 2008; Rothé et al., 2011). It might be that gamma band is a vehicle to encode outcome
606 expectation in a broad sense, with different regions encoding different dimensions (reward,
607 sensory feedback) of outcome expectancy. Indeed, these previous studies reported
608 modulation of gamma power in frontal regions during adaptation while we located it in post-
609 central regions. This assumption is neurophysiologically plausible as power in gamma band
610 is highly localized (e.g. Sirota et al., 2008), reflecting specific computations of local groups of
611 neurons in the neocortex. This calls for a more elaborated study on the extent to which
612 gamma-modulated oscillations contribute to recalibration of internal model and adaptive
613 behavior.

614 Another important finding of the present study was the implication of post-movement
615 synchrony of prefrontal, and to a lower extent premotor, theta oscillations in adaptive
616 learning. This finding is in line with the overall implication of the prefrontal cortex in the
617 coordination of adaptive goal-directed behavior (Koechlin, 2016; Miller et al., 2010;

Ridderinkhof et al., 2004), and also replicates the previous finding of a modulation of prefrontal theta power during visuomotor adaptation (Gentili et al., 2011; Perfetti et al., 2011). Although these latter studies have speculated on the role of theta enhancement in the formation of internal models, they were not designed to tease out whether it relates to changes in the state of the internal model that responds to error on a trial basis or to the accumulation of these changes over time to form a new mapping. The inclusion of a condition in which errors were random and equaled zero on average allowed us to specifically link the increase of prefrontal theta oscillatory activity to cumulative learning of the new sensorimotor mapping. This interpretation is in line with a large consensus about the implication of the prefrontal cortex, especially the ventromedial and lateral components, in encoding and learning predictive models mapping stimulus–action onto expected outcomes (Anguera et al., 2009; Contreras-Vidal and Kerick, 2004; Koechlin, 2016). There is also firm evidence that new acquired motor memories are stored and consolidated in prefrontal and secondary motor cortices (Dandolo and Schwabe, 2019; Pinsard et al., 2019). In particular, the ability to store newly learned behavior as memory-based constructs requires implementing top-down control signals from the prefrontal cortex to motor regions (Narayanan and Laubach, 2006), these latter regions being involved in selecting motor plans in response to stimuli (Koechlin et al., 2003). Finally, our interpretation is also consonant with a recent study having demonstrated that exploitation of learned associations between stimuli and responses during spatial context learning are implemented in prefrontal theta band activity (Spaak and de Lange, 2020).

Even though we have emphasized that our approach distinguished between oscillatory activity related to trial-to-trial changes in the internal model (i.e. adaptation) and oscillatory activity responsible for accumulating these changes across trials (i.e. learning), it is also possible that another process, namely cognitive strategy, has affected the study outcomes. It has been shown that individuals employ cognitive strategies to eliminate the error at the beginning of adaptive learning, and that implicit adaptation increasingly takes over from

explicit cognitive strategies as skill learning proceeds (Miyamoto et al., 2020; Taylor et al., 2014; Taylor and Ivry, 2011). Thus, our primary outcome on comparison between early and late stages of constant rotation condition (increase of power in theta, beta and gamma bands) could to some extent also reflect the change in the balance between explicit and implicit processes which are at work during adaptive learning. Individuals may have also employed explicit cognitive strategies to adapt in the random rotation condition, possibly affecting our secondary comparison between constant and random rotation conditions. There is evidence that explicit cognitive strategies influence sensorimotor adaptation even in conditions where perturbations are poorly predictable (Albert et al., 2021; Miyamoto et al., 2020). We have very few clues about the neural correlates of implicit and explicit processes in motor learning. To our knowledge, it has been proposed only recently that explicit cognitive and implicit processes are reflected into beta-band activities of distinct regions, the medial frontal region and the lateral central region, respectively (Jahani et al., 2020). Hence, SMA-related increase in beta power during the course of adaptation may not only reflect adaptive changes in the sensorimotor mapping but may also relate to a reduction of movement error guided by a cognitive strategy. It will be important for future studies to confirm that the increase in beta and theta band activities during adaptive learning are hallmarks of trial-to-trial adaptation error and cumulative learning of the new sensorimotor mapping and not a byproduct of the changes in the interactions between explicit strategy and implicit motor adaptation. This will require designing adaptive learning experiments that isolate as much as possible explicit and implicit processes of adaptation, for instance by delaying presentation of the feedback for the former (Brudner et al., 2016; Schween and Hegele, 2017) and limiting reaction time for the latter (Haith et al., 2015; Leow et al., 2017). Another solution to isolate the explicit component of adaptation may consist in asking subjects to report where they plan to aim before each trial (Miyamoto et al., 2020; Taylor et al., 2014). Finally, we cannot rule out the possibility that subjects exposed across trials to random variations in visuomotor transformation were able to learn some meta-parameters related to the multiple transformations; the so-called structural learning that fasters learning

673 in a new situation (Bond and Taylor, 2017; Braun et al., 2010). Hence, our conditions of
674 constant and random rotations may not have been perfectly orthogonal with respect to
675 learning of the new mapping.

676 Our results on the relationship between specific sensorimotor processes and particular
677 EEG bands and regions would not have been possible without a multi-band exploration of
678 the tasks through machine learning MKL modelling. This stresses how important it is to study
679 brain oscillations in adaptive learning, and more generally motor control, beyond beta band.
680 This complements previous observations that not only beta band but also other oscillatory
681 activities are important to enhance motor performance (Chung et al., 2017). In this
682 perspective, looking at the coupling between theta and gamma or beta is an important
683 challenge, such couplings coordinating communication across brain regions and contributing
684 to the formation of memory traces (Lisman and Jensen, 2013). In particular, it has been
685 shown that theta-gamma and theta-beta coupling can predict individual working memory
686 performance (Axmacher et al., 2010) which is known to be engaged in visuomotor adaptation
687 (Anguera et al., 2010; Christou et al., 2016). Closely related is the need to foster whole-brain
688 approaches that integrate not only the sensorimotor regions that have been traditionally
689 explored but also the frontal regions that likely generate theta oscillations. Some studies
690 suggested that dACC would process errors to output a control signal that specifies the need
691 for adjustments toward downstream regions, including the prefrontal cortex, responsible for
692 implementing corresponding adjustments (Ridderinkhof et al., 2004; Shenhav et al., 2016).
693 Given this assumption, investigating the coupling between prefrontal theta and SMA beta
694 oscillations could be valuable in the context of motor adaptation.

695 **5. Conclusion**

696 The current study advances our understanding of adaptive learning in humans by
697 demonstrating changes of oscillatory activity in multiple bands and regions and linking these
698 changes to specific “adaptive” and “learning” motor processes. Consistent with previous
699 studies, the results indicated that beta power, here of the supplementary motor area,

underpins error-dependent changes in trial-to-trial performance and as such reflects neural processes that evaluate motor error and likely signal a need for adaptation of the motor output. The other main outcome is the contribution of frontal theta power to adaptive learning, yet without being related to errors. This suggests a role of theta oscillations in storing the newly learned internal model. Whether these spatially and band-wise distinct oscillatory activities constitute neural correlates of implicit motor adaptation, only, or also reflect cognitive strategies that may operate during motor adaptation to learn from errors remains to be tested.

6. Data and code availability statement

All raw data are stored on SUMMER, the data server of Grenoble-Alpes university and will be made available without restrictions upon request to lucas.struber@univ-grenoble-alpes.fr or fabien.cignetti@univ-grenoble-alpes.fr. Analysis codes can be found on gitlab, at the following address https://gricad-gitlab.univ-grenoble-alpes.fr/lstruber-research.

7. Acknowledgments

This work was supported by the French National Research Agency in the framework of the “Investissements d’avenir” program (ANR-15-IDEX-02). The authors declare no competing financial interest.

References

Alayrangues, J., Torrecillos, F., Jahani, A., Malfait, N., 2019. Error-related modulations of the sensorimotor post-movement and foreperiod beta-band activities arise from distinct neural substrates and do not reflect efferent signal processing. Neuroimage 184, 10–24. https://doi.org/10.1016/j.neuroimage.2018.09.013

Albert, S.T., Jang, J., Sheahan, H.R., Teunissen, L., Vandevoorde, K., Herzfeld, D.J., Shadmehr, R., 2021. An implicit memory of errors limits human sensorimotor adaptation. Nat. Hum. Behav. 2, 1–38. https://doi.org/10.1038/s41562-020-01036-x

Amiez, C., Hadj-Bouziane, F., Petrides, M., 2012. Response selection versus feedback analysis in conditional visuo-motor learning. Neuroimage 59, 3723–3735. https://doi.org/10.1016/j.neuroimage.2011.10.058

Anguera, J.A., Reuter-Lorenz, P.A., Willingham, D.T., Seidler, R.D., 2010. Contributions of spatial working memory to visuomotor adaptation. J. Cogn. Neurosci. 22, 1917–1930. https://doi.org/10.1162/jocn.2009.21351

Anguera, J.A., Seidler, R.D., Gehring, W.J., 2009. Changes in performance monitoring during sensorimotor adaptation. J. Neurophysiol. 102, 1868–1879. https://doi.org/10.1152/jn.00063.2009

Axmacher, N., Henseler, M.M., Jensen, O., Weinreich, I., Elger, C.E., Fell, J., 2010. Cross-frequency coupling supports multi-item working memory in the human hippocampus. Proc. Natl. Acad. Sci. 107, 3228–3233. https://doi.org/10.1073/pnas.0911531107

Bond, K.M., Taylor, J.A., 2017. Structural learning in a visuomotor adaptation task is explicitly accessible. eNeuro 4, 1–16. https://doi.org/10.1523/ENEURO.0122-17.2017

Bonini, F., Burle, B., Liégeois-Chauvel, C., Régis, J., Chauvel, P., Vidal, F., 2014. Action monitoring and medial frontal cortex: Leading role of supplementary motor area. Science (80-.). 343, 888–891. https://doi.org/10.1126/science.1247412

743 Botvinick, M.M., Cohen, J.D., Carter, C.S., 2004. Conflict monitoring and anterior cingulate
744 cortex: An update. Trends Cogn. Sci. 8, 539–546.
745 https://doi.org/10.1016/j.tics.2004.10.003

746 Braun, D.A., Aertsen, A., Wolpert, D.M., Mehring, C., 2009a. Learning optimal adaptation
747 strategies in unpredictable motor tasks. J. Neurosci. 29, 6472–6478.
748 https://doi.org/10.1523/JNEUROSCI.3075-08.2009

749 Braun, D.A., Aertsen, A., Wolpert, D.M., Mehring, C., 2009b. Motor Task Variation Induces
750 Structural Learning. Curr. Biol. 19, 352–357. https://doi.org/10.1016/j.cub.2009.01.036

751 Braun, D.A., Mehring, C., Wolpert, D.M., 2010. Structure learning in action. Behav. Brain
752 Res. 206, 157–165. https://doi.org/10.1016/j.bbr.2009.08.031

753 Brovelli, A., Ding, M., Ledberg, A., Chen, Y., Nakamura, R., Bressler, S.L., 2004. Beta
754 oscillations in a large-scale sensorimotor cortical network: Directional influences
755 revealed by Granger causality. Proc. Natl. Acad. Sci. 101, 9849–9854.
756 https://doi.org/10.1073/pnas.0308538101

757 Brudner, S.N., Kethidi, N., Graeupner, D., Ivry, R.B., Taylor, J.A., 2016. Delayed feedback
758 during sensorimotor learning selectively disrupts adaptation but not strategy use. J.
759 Neurophysiol. 115, 1499–1511. https://doi.org/10.1152/jn.00066.2015

760 Bruns, A., 2004. Fourier-, Hilbert- and wavelet-based signal analysis: Are they really different
761 approaches? J. Neurosci. Methods 137, 321–332.
762 https://doi.org/10.1016/j.jneumeth.2004.03.002

763 Christou, A.I., Miall, R.C., McNab, F., Galea, J.M., 2016. Individual differences in explicit and
764 implicit visuomotor learning and working memory capacity. Sci. Rep. 6, 1–13.
765 https://doi.org/10.1038/srep36633

766 Chung, J.W., Ofori, E., Misra, G., Hess, C.W., Vaillancourt, D.E., 2017. Beta-band Activity
767 and Connectivity in Sensorimotor and Parietal Cortex are Important for Accurate Motor

768 Performance. Neuroimage 144, 164–173.
769 https://doi.org/10.1016/j.neuroimage.2016.10.008

770 Cohen, M.X., Elger, C.E., Fell, J., 2009. Oscillatory activity and phase-amplitude coupling in
771 the human medial frontal cortex during decision making. J. Cogn. Neurosci. 21, 390–
772 402. https://doi.org/10.1162/jocn.2008.21020

773 Combrisson, E., Perrone-Bertolotti, M., Soto, J.L.P., Alamian, G., Kahane, P., Lachaux, J.P.,
774 Guillot, A., Jerbi, K., 2017. From intentions to actions: Neural oscillations encode motor
775 processes through phase, amplitude and phase-amplitude coupling. Neuroimage 147,
776 473–487. https://doi.org/10.1016/j.neuroimage.2016.11.042

777 Contreras-Vidal, J.L., Kerick, S.E., 2004. Independent component analysis of dynamic brain
778 responses during visuomotor adaptation. Neuroimage 21, 936–945.
779 https://doi.org/10.1016/j.neuroimage.2003.10.037

780 Cortes, C., Vapnik, V., 1995. Support-Vector Networks. Mach. Learn. 273–297.
781 https://doi.org/10.1007/BF00994018

782 Dandolo, L.C., Schwabe, L., 2019. Time-dependent motor memory representations in
783 prefrontal cortex. Neuroimage 197, 143–155.
784 https://doi.org/10.1016/j.neuroimage.2019.04.051

785 Delorme, A., Sejnowski, T., Makeig, S., 2007. Enhanced Detection of Artifacts in EEG Data
786 using Higher-order Statistics and Independent Component Analysis. Neuroimage 34,
787 1443–1449. https://doi.org/10.1016/j.neuroimage.2006.11.004

788 Diedrichsen, J., Hashambhoy, Y., Rane, T., Shadmehr, R., 2005. Neural correlates of reach
789 errors. J. Neurosci. 25, 9919–9931. https://doi.org/10.1523/JNEUROSCI.1874-05.2005

790 Donchin, O., Francis, J.T., Shadmehr, R., 2003. Quantifying generalization from trial-by-trial
791 behavior of adaptive systems that learn with basis functions: Theory and experiments in
792 human motor control. J. Neurosci. 23, 9032–9045. https://doi.org/10.1523/jneurosci.23-

27-09032.2003

Gentili, R.J., Bradberry, T.J., Oh, H., Hatfield, B.D., Contreras Vidal, J.L., 2011. Cerebral cortical dynamics during visuomotor transformation: Adaptation to a cognitive-motor executive challenge. Psychophysiology 48, 813–824. https://doi.org/10.1111/j.1469-8986.2010.01143.x

Gönen, M., Alapydin, E., 2011. Multiple Kernel Learning Algorithms. J. Mach. Learn. Res. 12, 2211–2268.

Haith, A.M., Huberdeau, D.M., Krakauer, J.W., 2015. The influence of movement preparation time on the expression of visuomotor learning and savings. J. Neurosci. 35, 5109–5117. https://doi.org/10.1523/JNEUROSCI.3869-14.2015

Hammer, J., Fischer, J., Ruescher, J., Schulze-bonhage, A., Aertsen, A., Mcfarland, D.J., 2013. The role of ECoG magnitude and phase in decoding position , velocity , and acceleration during continuous motor behavior. Front. Neurosci. 7, 200. https://doi.org/10.3389/fnins.2013.00200

Haynes, J.D., 2015. A Primer on Pattern-Based Approaches to fMRI: Principles, Pitfalls, and Perspectives. Neuron 87, 257–270. https://doi.org/10.1016/j.neuron.2015.05.025

Jahani, A., Schwey, A., Bernier, P.M., Malfait, N., 2020. Spatially distinct beta-band activities reflect implicit sensorimotor adaptation and explicit re-aiming strategy. J. Neurosci. 40, 2498–2509. https://doi.org/10.1523/JNEUROSCI.1862-19.2020

Jerbi, K., Lachaux, J., Diaye, K.N., Pantazis, D., Leahy, R.M., Garnero, L., Baillet, S., 2007. Coherent neural representation of hand speed in humans revealed by MEG imaging. Proc. Natl. Acad. Sci. 104, 7676–7681. https://doi.org/10.1073/pnas.0609632104

Kilavik, B.E., Zaepffel, M., Brovelli, A., MacKay, W.A., Riehle, A., 2013. The ups and downs of beta oscillations in sensorimotor cortex. Exp. Neurol. 245, 15–26. https://doi.org/10.1016/j.expneurol.2012.09.014

818 Koechlin, E., 2016. Prefrontal executive function and adaptive behavior in complex
819 environments. Curr. Opin. Neurobiol. 37, 1–6.
820 https://doi.org/10.1016/j.conb.2015.11.004

821 Koechlin, E., Ody, C., Kouneiher, F., 2003. The Architecture of Cognitive Control in the
822 Human Prefrontal Cortex. Science (80-.). 302, 1181–1185.
823 https://doi.org/10.1126/science.1088545

824 Kriegeskorte, N., Simmons, W.K., Bellgowan, P.S.F., Baker, C.I., 2009. Circular analysis in
825 systems neuroscience – the dangers of double dipping. Nat. Neurosci. 12, 535–540.
826 https://doi.org/https://doi.org/10.1038/nn.2303

827 Leow, L.A., Gunn, R., Marinovic, W., Carroll, T.J., 2017. Estimating the implicit component of
828 visuomotor rotation learning by constraining movement preparation time. J.
829 Neurophysiol. 118, 666–676. https://doi.org/10.1152/jn.00834.2016

830 Lisman, J.E., Jensen, O., 2013. The Theta-Gamma Neural Code, Neuron.
831 https://doi.org/10.1016/j.neuron.2013.03.007

832 Miller, K.J., Schalk, G., Fetz, E.E., den Nijs, M., Ojemann, J.G., Rao, R.P.N., 2010. Cortical
833 activity during motor execution, motor imagery, and imagery-based online feedback.
834 Proc. Natl. Acad. Sci. 107, 4430–4435. https://doi.org/10.1073/pnas.0913697107

835 Miyamoto, Y.R., Wang, S., Smith, M.A., 2020. Implicit adaptation compensates for erratic
836 explicit strategy in human motor learning. Nat. Neurosci. 23, 443–455.
837 https://doi.org/10.1038/s41593-020-0600-3

838 Muthukumaraswamy, S.D., 2010. Functional properties of human primary motor cortex
839 gamma oscillations. J. Neurophysiol. 104, 2873–2885.
840 https://doi.org/10.1152/jn.00607.2010

841 Narayanan, N.S., Laubach, M., 2006. Top-down control of motor cortex ensembles by
842 dorsomedial prefrontal cortex. Neuron 52, 921–931.

https://doi.org/https://doi.org/10.1016/j.neuron.2006.10.021

Noirhomme, Q., Lesenfants, D., Gomez, F., Soddu, A., Schrouff, J., Garraux, G., Luxen, A., Phillips, C., Laureys, S., 2014. Biased binomial assessment of cross-validated estimation of classification accuracies illustrated in diagnosis predictions. NeuroImage Clin. 4, 687–694. https://doi.org/10.1016/j.nicl.2014.04.004

Nowak, M., Zich, C., Stagg, C.J., 2018. Motor Cortical Gamma Oscillations: What Have We Learnt and Where Are We Headed? Curr. Behav. Neurosci. Reports 5, 136–142. https://doi.org/10.1007/s40473-018-0151-z

Ojala, M., Garriga, G.C., 2010. Permutation tests for studying classifier performance. J. Mach. Learn. Res. 11, 1833–1863.

Palmer, C.E., Auksztulewicz, R., Ondobaka, S., Kilner, J.M., 2019. Sensorimotor beta power reflects the precision-weighting afforded to sensory prediction errors. Neuroimage 200, 59–71. https://doi.org/10.1016/j.neuroimage.2019.06.034

Pereira, F., Mitchell, T., Botvinick, M., 2009. Machine learning classifiers and fMRI: a tutorial overview. Neuroimage 45, S199–S209. https://doi.org/10.1016/j.neuroimage.2008.11.007

Perfetti, B., Moisello, C., Landsness, E.C., Kvint, S., Lanzafame, S., Onofrj, M., Rocco, A. Di, Tononi, G., Ghilardi, M.F., 2011. Modulation of Gamma and Theta Spectral Amplitude and Phase Synchronization Is Associated with the Development of Visuo-Motor Learning. J. Neurosci. 31, 14810–14819. https://doi.org/10.1523/JNEUROSCI.1319-11.2011

Pinsard, B., Boutin, A., Gabitov, E., Lungu, O., Benali, H., Doyon, J., 2019. Consolidation alters motor sequence- specific distributed representations. Elife 8, 1–20. https://doi.org/10.7554/eLife.39324

Popovych, S., Rosjat, N., Toth, T.I., Wang, B.A., Liu, L., Abdollahi, R.O., Viswanathan, S.,

868 Grefkes, C., Fink, G.R., Daun, S., 2016. Movement-related phase locking in the delta–
869 theta frequency band. Neuroimage 139, 439–449.
870 https://doi.org/10.1016/j.neuroimage.2016.06.052

871 Rakotomamonjy, A., Bach, F.R., Canu, S., Grandvalet, Y., 2008. SimpleMKL. J. Mach.
872 Learn. Res. 9, 2491–2521.

873 Ridderinkhof, K.R., Ullsperger, M., Crone, E.A., Nieuwenhuis, S., 2004. The role of the
874 medial frontal cortex in cognitive control. Science (80-.). 306, 443–447.
875 https://doi.org/10.1126/science.1100301

876 Schrouff, J., Mourão-Miranda, J., Phillips, C., Parvizi, J., 2016. Decoding intracranial EEG
877 data with multiple kernel learning method. J. Neurosci. Methods 261, 19–28.
878 https://doi.org/10.1016/j.jneumeth.2015.11.028

879 Schween, R., Hegele, M., 2017. Feedback delay attenuates implicit but facilitates explicit
880 adjustments to a visuomotor rotation. Neurobiol. Learn. Mem. 140, 124–133.
881 https://doi.org/10.1016/j.nlm.2017.02.015

882 Shenhav, A., Cohen, J.D., Botvinick, M.M., 2016. Dorsal anterior cingulate cortex and the
883 value of control. Nat. Neurosci. 19, 1286–1291. https://doi.org/10.1038/nn.4384

884 Sirota, A., Montgomery, S., Fujisawa, S., Isomura, Y., Zugaro, M., Buzsáki, G., 2008.
885 Entrainment of Neocortical Neurons and Gamma Oscillations by the Hippocampal Theta
886 Rhythm. Neuron 60, 683–697. https://doi.org/10.1016/j.neuron.2008.09.014

887 Spaak, E., de Lange, F.P., 2020. Hippocampal and prefrontal theta-band mechanisms
888 underpin implicit spatial context learning. J. Neurosci. 40, 191–202.
889 https://doi.org/10.1523/JNEUROSCI.1660-19.2019

890 Tan, H., Jenkinson, N., Brown, P., 2014a. Dynamic neural correlates of motor error
891 monitoring and adaptation during trial-to-trial learning. J. Neurosci. 34, 5678–5688.
892 https://doi.org/10.1523/JNEUROSCI.4739-13.2014

Tan, H., Wade, C., Brown, P., 2016. Post-movement beta activity in sensorimotor cortex indexes confidence in the estimations from internal models. J. Neurosci. 36, 1516–1528. https://doi.org/10.1523/JNEUROSCI.3204-15.2016

Tan, H., Zavala, B., Pogosyan, A., Ashkan, K., Zrinzo, L., Foltynie, T., Limousin, P., Brown, P., 2014b. Human subthalamic nucleus in movement error detection and its evaluation during visuomotor adaptation. J. Neurosci. 34, 16744–16754. https://doi.org/10.1523/JNEUROSCI.3414-14.2014

Taylor, J.A., Ivry, R.B., 2011. Flexible cognitive strategies during motor learning. PLoS Comput. Biol. 7. https://doi.org/10.1371/journal.pcbi.1001096

Taylor, J.A., Krakauer, J.W., Ivry, R.B., 2014. Explicit and implicit contributions to learning in a sensorimotor adaptation task. J. Neurosci. 34, 3023–3032. https://doi.org/10.1523/JNEUROSCI.3619-13.2014

Thürer, B., Weber, F.D., Born, J., Stein, T., 2018. Variable training but not sleep improves consolidation of motor adaptation. Sci. Rep. 8, 15977. https://doi.org/10.1038/s41598-018-34225-w

Torrecillos, F., Alayrangues, J., Kilavik, B.E., Malfait, N., 2015. Distinct modulations in sensorimotor postmovement and foreperiod $β$-band activities related to error salience processing and sensorimotor adaptation. J. Neurosci. 35, 12753–12765. https://doi.org/10.1523/JNEUROSCI.1090-15.2015

Tzagarakis, C., Ince, N.F., Leuthold, A.C., Pellizzer, G., 2010. Beta-band activity during motor planning reflects response uncertainty. J. Neurosci. 30, 11270–11277. https://doi.org/10.1523/JNEUROSCI.6026-09.2010

Voytek, B., D'Esposito, M., Crone, N., Knight, R.T., 2013. A Method for Event-related Phase/Amplitude Coupling. Neuroimage 64, 416–424. https://doi.org/10.1016/j.neuroimage.2012.09.023

Wolpert, D.M., Ghahramani, Z., Jordan, M.I., 1995. An Internal Model for Sensorimotor Integration. Science (80-.). 269, 1880–1882. https://doi.org/10.1126/science.7569931

Wolpert, D.M., Miall, R.C., 1996. Forward Models for Physiological Motor Control. Neural Networks 9, 1265–1279. https://doi.org/10.1016/s0893-6080(96)00035-4